Journal of
Materials Chemistry C

Materials for optical, magnetic and electronic devices

Accepted Manuscript

This article can be cited before page numbers have been issued, to do this please use: Y. Liu, X. Wei, Y. Chen, Y. Yang, Y. Zhang and H. Liu, *J. Mater. Chem. C*, 2025, DOI: 10.1039/D5TC02438B.

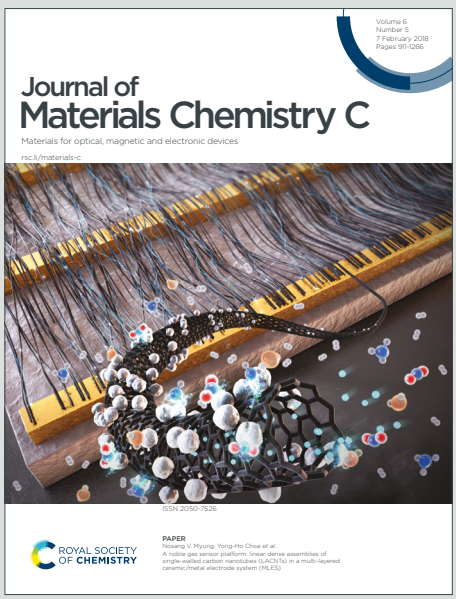

ROYAL SOCIETY OF CHEMISTRY

rsc.li/materials-c

View Article Online
DOI: 10.1039/D5TC02438B

Assembly of Intrinsic Chiral Gold Nanorods within a Cholesteric Liquid Crystal Host with the Tunable Optical Asymmetry

Yang Liu[1,*], Xiyang Wei[1], Yongguang Chen[1], Yi Yang[1], Yongfang Zhang[1], Hao Liu[1]

1. College of Information Science and Technology, Donghua University, 2999 North Renmin Road, Songjiang District, Shanghai 201-620, China.

Email: liuyang@dhu.edu.cn

Abstract: A recent upsurge of interest has been observed in exploring the chiral nature of nanomaterials and their assembly. In this work, we conducted theoretical investigations into the optical asymmetry of chiral gold nanorods (c-Au NRs) helical assemblies within a cholesteric liquid crystal (CLC) host. The research investigated the optical asymmetry of the assemblies from two perspectives: the enhanced optical asymmetry of the helical assemblies due to the chiral nature of the c-Au NRs, and the sufficient dynamic modulation ways of the optical asymmetry by tuning the geometrical properties of the helical assemblies. In the context of post-modulation, the azimuthal variation has been identified as the most effective factor with a range of 0 to $\pi/3$ resulting in a change in the g-factor up to 0.271, indicating a broaden modulation range by 44.72% at its original base. The silver shell on Au NRs has been observed to strongly blue-shift the optical asymmetric signal of the helical assemblies, but concurrently reduces the amplitudes. The findings presented herein not only demonstrate the ground truth method raising the optical symmetry of c-Au NRs helical assemblies, but also indicates the pathway toward magnifying and dynamically tuning the optical asymmetry in a large scale.

Keywords: Gold Nanorods, Helical Assembly, Cholesteric Liquid Crystals, Optical Asymmetry

Introduction

Chirality is a fundamental property of matter, manifesting as a natural phenomenon in numerous biological and chemical systems [1-3]. In comparison to the natural chiral macro- or nano-structures, the artificial assemblies with the designed chiral properties are of significant value in a number of applications, including optical signal processing [4], chiral molecule recognition [5-6], photothermal therapy [7], biosensing [8], and others. The exploration of methods to enhance and modulate the chirality of these assemblies is a crucial aspect of their exploitation. Plasmonic nanostructures with notable light-matter interactions have emerged as a key component in the creation of chiral assemblies. Among the various plasmonic nanomaterials, anisotropic gold nanorods (Au NRs), which exhibit dual tunable localized surface plasmon resonance (LSPR) in their longitudinal and transverse directions [9], have been identified as a valuable component for the fabrication of assemblies, integrating the functionality of the bulk with additional tunable properties.

The template-assisted bottom-up method has been utilized to investigate both 2D and 3D Au NRs helical assemblies. A chiral hybrid superstructure has been previously demonstrated through a hierarchical, cooperative self-assembly/self-organization process in a multiple-component system comprising gold nanorods, surfactants, and

phospholipid film [10-14]. The chirality of the fabricated Au NRs helical assemblies has been confirmed by circular dichroism spectrum, and the helical alignment of Au NRs in the hybrid superstructure would resemble mesogenic molecules in a cholesteric liquid crystalline mesophase, with the Coulomb dipole–dipole interactions between gold nanorods in such a chiral liquid crystalline-like mesophase giving rise to the plasmonic circular dichroism effect [15]. Furthermore, evidence has been found that long-range organization of Au NRs in a manner similar to liquid crystals (LCs) has been established with human islet amyloid polypeptides, and a strong, polarization-dependent spectral shift and the reduced scattering of energy states with antiparallel orientation of dipoles activated in assembled helices has increased optical asymmetry g-factors by a factor of more than 4600 [16]. Nevertheless, the chiral characteristics of these Au NRs helical assemblies are significantly dependent on the templates, and in rare cases the geometry of Au NRs helical assemblies can be modified by processing temperature, light illumination, PH and electromagnetic field [17-21]. The dynamic modulation of chiral characteristics remains a challenging. LCs are an optimal host matrix for the assembly of nanomaterials, and offer the assemblies the potential to dynamically tune their geometries by pitch, inter-nanorod space and orientation [22-24]. The successful preparation of strip and helical assemblies in a LC host has been previously demonstrated [25], and in a recent study we reported the helical assembly of Au NRs in a cholesteric liquid crystal (CLC) host, demonstrating dynamic tuning of the helical assemblies via UV-triggered processes [26]. However, due to the limited oscillation of the illuminant polarized light around the helical assemblies, their optical asymmetry change in response to the dynamic geometry modulation is not significant, which is contrary to the desired results.

Compared to normal Au NRs, the additional artificial intrinsic chirality on Au NRs has been shown to enhance the oscillation of the polarized light of the illuminant [27, 28]. The intrinsically chiral Au NRs (c-Au NRs) are a previous alternative of normal Au NRs in helical assemblies to achieve a high optical asymmetry [29-31]. However, the fabrication of chiral geometry on the surface of Au NRs, especially the programmable fabrication of fine nano-architectures on Au NRs is extremely difficult. In this research, we used computer-aided design technology to fabricate c-Au NRs and theoretically study their geometry-dependent intrinsic chirality by means of FDTD simulation, and then we tried to fabricate helical assemblies in a CLC host and study the intrinsic chirality transformation of c-Au NRs into helical assemblies. We proposed the method in fabricating highly optically asymmetric c-Au NRs helical assemblies and revealed the modulation rules of optical asymmetry in helical assemblies from the aspect of inter-nanorod space, azimuthal variations and rotation in both side-by-side fashion and end-to-end fashion.

Results and Discussion

The extinction of Au NRs is inherently anisotropic in both the longitudinal and transverse directions. Our previous study demonstrated that reducing the distance between Au NRs and incorporating the additional Au NRs in helical assemblies resulted in a decrease in the longitudinal extinction signals and an increase in the transverse extinction signals, as well as the increase in CD signals and g-factors. We believe the anisotropy in the extinction of Au NRs is an essential sign to understand the chiral characteristics of Au NRs and their assemblies, and here we determine an extinction anisotropy factor (Δe) of Au NRs and their assemblies as followings to evaluate their chiral characteristics,

$$\Delta e = 1 - \frac{|e_L - e_T|}{e_L + e_T}, \quad (1)$$

where e_L is the intensity of longitudinal extinction signal, and e_T is the intensity of transverse extinction signal. Therefore, when the Au NRs are longitudinally perpendicular to the polarization direction of the incident light, it means that in the extinction spectra $e_L > e_T$, we will have

View Article Online
DOI: 10.1039/D5TC02438B

$$\Delta e = \frac{2e_T}{e_L+e_T}, \quad (2)$$

and when the Au NRs are longitudinally parallel to the polarization direction of the incident light, it means that in the extinction spectra $e_T > e_L$, we will have

$$\Delta e = \frac{2e_L}{e_L+e_T}. \quad (3)$$

Therefore, Δe is in the range 0-1, and the Δe approaching to 1 indicates that an extremely large extinction anisotropy in Au NRs. To further verify the generality and applicability of the proposed Δe in relation to chiral characteristics, the extinction, CD, g-factor characteristics of 29 different Au NRs with different aspect ratios and their corresponding helical assemblies in a CLCs host were simulated under different pitches. The resulting curve relationship between the Δe and the asymmetric g-factor is shown in **Fig. 1**. The simulation results demonstrate that, for both Au NRs with different aspect ratios and the corresponding helical assemblies, an increase in optical asymmetry value is accompanied by an increase in the asymmetric g-factor corresponding to each pitch, which is strongly consistent with our expectations. It can therefore be concluded that the Δe is general and universal, and can be further extended to the characterization of optical asymmetry of c-Au NRs, and we always have

$$\mathrm{g-factor} \sim \Delta e = 1 - \frac{|e_L - e_T|}{e_L+e_T}. \quad (4)$$

In this way, we employed the Δe to assess the chiral characteristics of c-Au NRs from the perspectives of rotational segments and twist angle, with the objective of identifying the most suitable c-Au NRs for the fabrication of helical assemblies exhibiting dynamically tunable optical asymmetries. In addition to the well-known wrinkled surface of c-Au NRs, the intrinsic chiral characteristics of these nanorods were firstly evaluated from the perspective of the twist angle, as illustrated in **Fig. S1**. The Au NRs (aspect ratio by 3.73, 56 nm in length ×15nm in diameter) are longitudinally divided into 1000 units in order to facilitate the smooth absorption of the twisting force and to enable them to withstand the formation of surface wrinkles. As shown in **Fig. S1a**, it was observed that the increase of the twist angle on c-Au NRs had a negligible impact on their surface morphology and volume, and the volume of the c-Au NR remains at approximately 100% until the twist angle reaches 6π. As the volume of Au NRs is a significant indicator of their extinction characteristics, the extinction spectra of c-Au NRs were confirmed to remain largely unchanged, with their transverse LSPR (t-LSPR) signals located at ~507 nm and longitudinal LSPR (l-LSPR) signals located at ~932 nm (**Fig. S1c,d**). Despite the minimal volume alteration of c-Au NRs and the largely unchanged extinction characteristics, a slight fluctuation in Δe is evidently seen from **Fig. S1e**. It can be seen that a reduction in Δe becomes apparent when the twist angle reaches 5π/4 and the lowest recorded value of Δe is observed at 4π twisting, after which it recovers to its initial high level at 11π/5. These results demonstrate that the slight change in Δe is negatively caused by twisting Au NRs, and greatly is in stark contrast to the findings reported in the recent literatures [26].

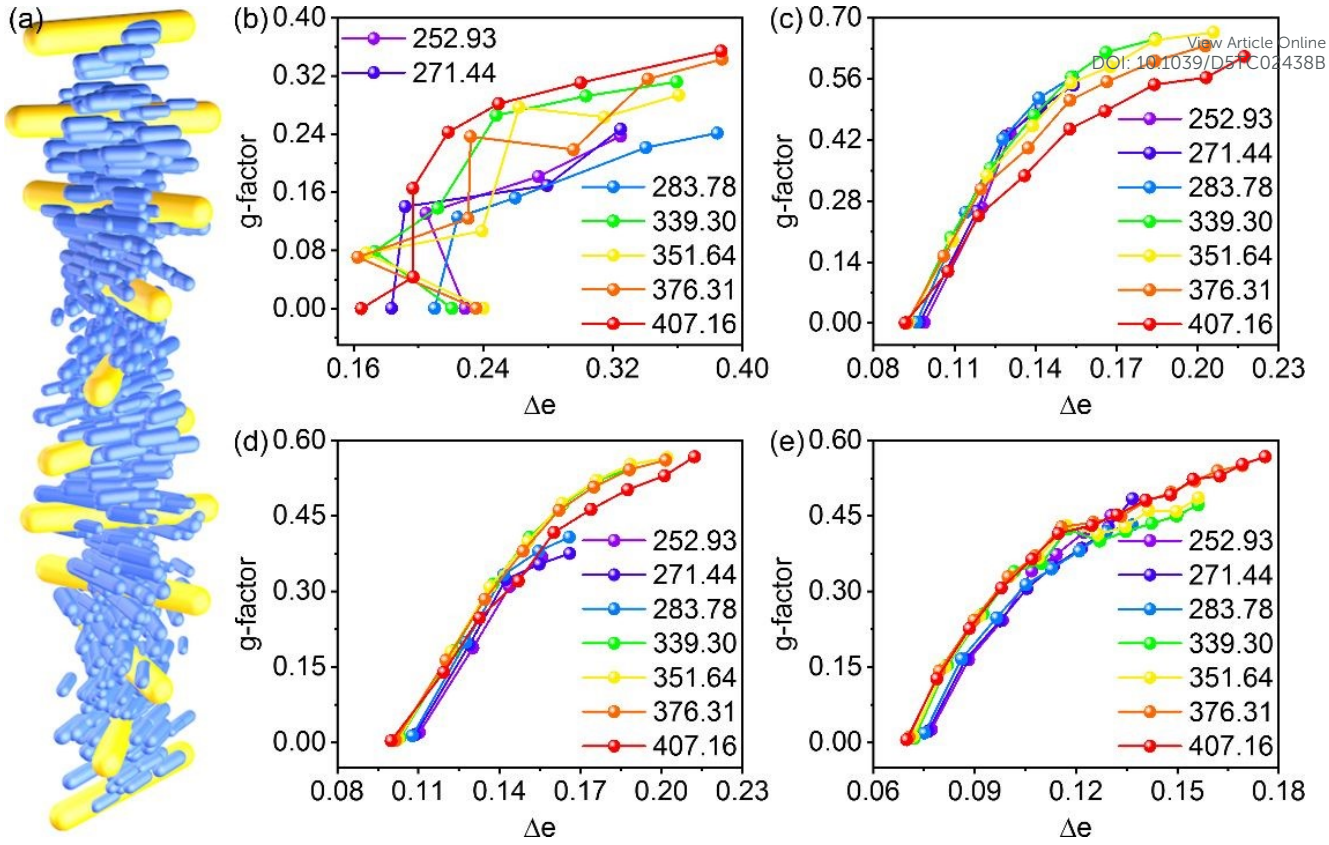

Fig. 1. (a) is the schematic of a 11-Au NRs helical assembly in the CLC-host. The g-factor of Au NRs helical assemblies as illustrated in (b), (c), (d) and (e) is contingent on the pitch of the helical assembly and the aspect ratio of the Au NRs, and the aspect ratio of Au NRs in (b), (c), (d) and (e) is 2.5 (40 nm in length ×16 nm in diameter), 3.9 (78 nm in length × 20 nm in diameter), 5.05 (101 nm in length × 20 nm in diameter) and 6.73 (101 nm in length × 15 nm in diameter), respectively.

In addition to the rotational segment, which is defined as the artificial equal-fractions at the tips of the gold nanorods. The c-Au NRs with 4 rotational segments are in cubic bar shape as shown in **Fig. S2a**, and it is seen that as the number of rotation segments was increased, the c-Au NRs became more rounded in shape and the corresponding volume increased gradually (**Fig. S2b**). When the rotational segments reach 15, the fabricated c-Au NRs exhibit a volume that is approaching to that of the normal one. As with the aforementioned results, the extinction spectra of the c-Au NRs with regard to the increase of rotational segment, is found to exhibit a gradual blue shift and increase in intensity due to their inherent volume-extinction characteristics as shown in **Fig. S2c,d.** The extinction anisotropy change was evaluated in relation to the rotation segments by referencing the intensities of the t-LSPR and l-LSPR signals, and it can be seen that due to the notable expansion of the l-LSPR signals and minimal alteration of the t-LSPR signals with respect to increasing rotational segments result in a remarkable increase of the Δe as shown in **Fig. S2e**. This indicates that the increase of rotation segments in c-Au NRs will induce the enhancement of their intrinsic chiral characteristics.

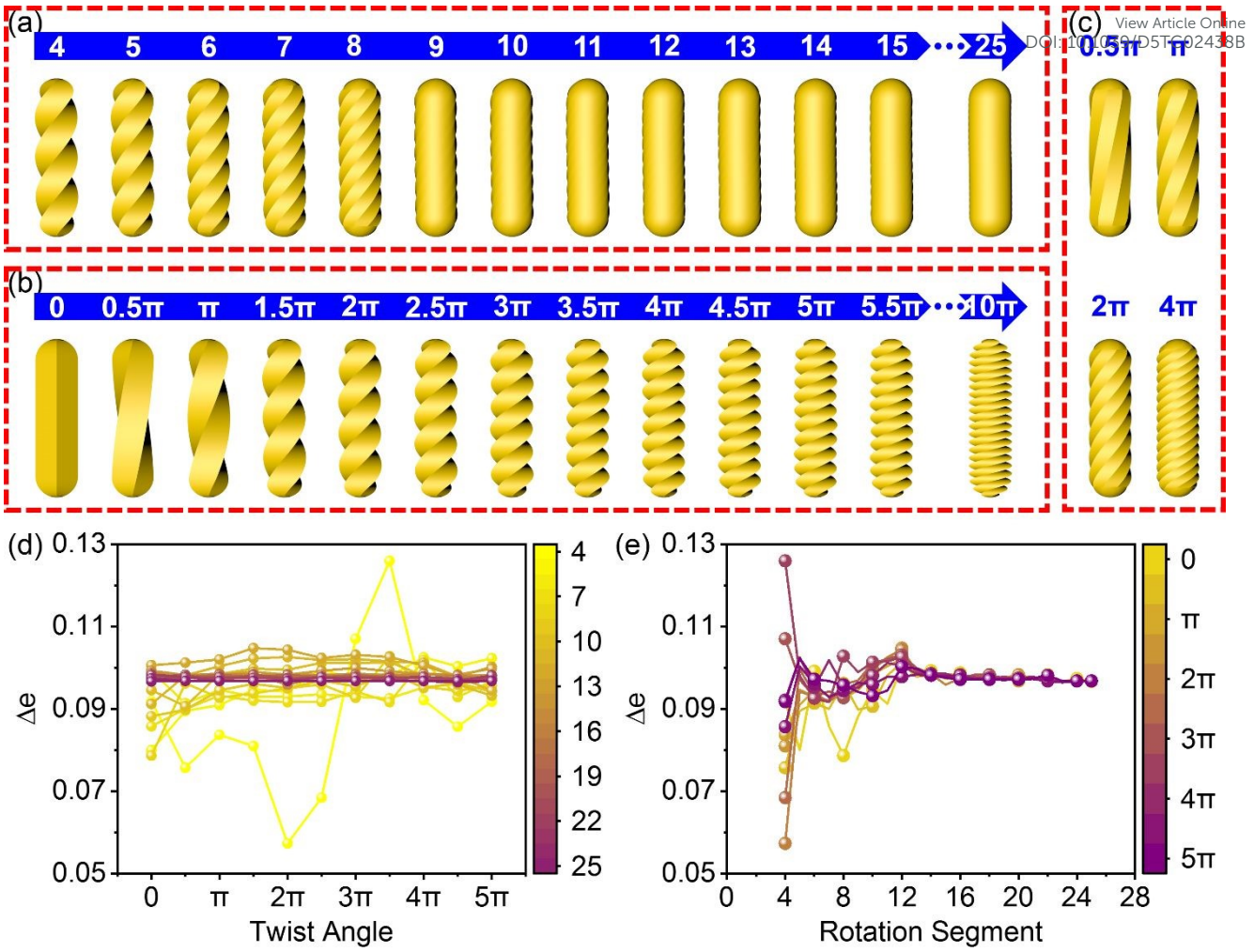

Fig. 2. (a) The function of the rotational segment on the Au NRs (aspect ratio by 3.73, 56 nm in length ×15 nm in diameter) with an intrinsic twist angle of 2π. The function of the twist angle on the Au NRs with an intrinsic rotational segment of (b) 4 and (c) 8. The correspondingly calculated Δe according to equation 2 as a function of (d) twist angle and (e) rotational segment.

Although the rotation segment and twist angle of a c-Au NR contribute to the tuning of its chiral characteristics, neither the twist angle nor the rotational segment visibly distinguish a programmable Au NR from a normal one in their optical asymmetric view. Furthermore, the combined function of these two parameters remains less well-defined. Accordingly, the combined function between the twist angle and the rotational segment is being investigated with regard to the morphological alteration of the Au NRs and the corresponding optical asymmetry. As illustrated in **Fig. 2a,b**, the dual functions of twist angle and rotational segments on Au NRs resulted in the typical observed wrinkles on the surface, and the wrinkles became narrower as the twist angle or rotational segments increase. By comparing the c-Au NRs twisted with the same angle but in 4 rotational segments and 8 rotational segments as shown in **Fig. 2b,c**, it was observed that a large number of rotational segments was able to induce a greater number of narrower wrinkles on Au NRs, resulting in a more rounded appearance. The modification of the volume of Au NRs by dual function between twist angle and rotational segments results in alterations to the extinction characteristics of the fabricated c-Au NRs and the accompanying extinction anisotropy. The variation in Δe in response to the twist angle at a given rotational segment is shown in **Fig. 2d**, and it can be observed that when the Au NR is modulated with 4 rotational segments, there is a significant fluctuation in Δe with the highest value of 0.1298 attained at the twist angle of 7π/2. As the number of rotational segments is increased continuously, the fluctuation of Δe in response to the twist angle is reduced, although there is an overall increase in Δe, and the

greatest Δe is typically observed at a twist angle of either $3\pi/2$ or 2π. The increase in Δe due to rotational segments is observed to decline when the rotational segments get as many as 12, indicating that a polygon-shaped c-Au NR is preferable for achieving high extinction anisotropy compared to a round one. This phenomenon is particularly evident in **Fig. 2e**, which demonstrates that when the number of rotational segments reach 12, all the c-Au NRs with different twist angles exhibit a similar Δe. The observed increase in Δe can be attributed to the rise in charge oscillations caused by wrinkles, and the fusion effect of the twist angle and rotational segments has been demonstrated to be an effective means of generating intrinsic chirality in c-Au NRs.

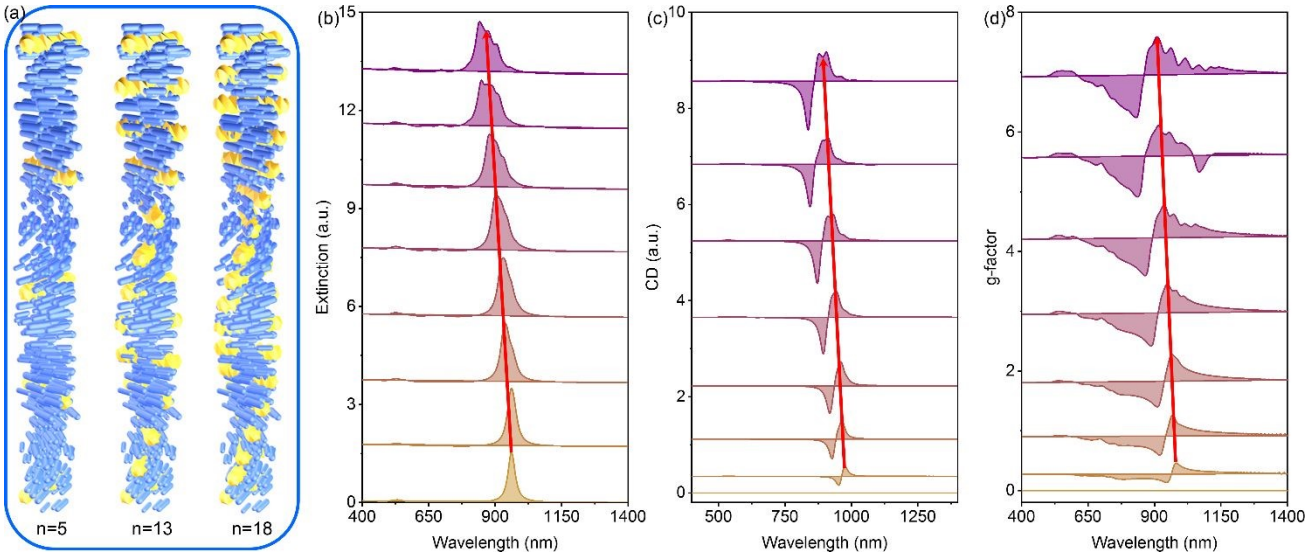

Fig. 3. (a) The schematics of a 407.16 nm helical assembly includes 5, 13 and 18 c-Au NRs (aspect ratio by 3.73, 56 nm in length ×15 nm in diameter), and (b-d) the changes in optical asymmetry that are caused by incorporating c-Au NRs into the helical assembly by 5, 7, 9, 11, 13, 15, 17, 18, respectively.

Table 1. Changes in the wavelengths of l-LSPR signals that are caused by the incorporation of c-Au NRs (aspect ratio by 3.73, 56 nm in length ×15 nm in diameter) into the helical assembly.

Helical Assembly	Au NRs		c-Au NRs	
	λ_{l-LSPR}	△	λ_{l-LSPR}	△
5	1.5343	NA	1.1224	NA
7	1.7769	0.2426	1.3215	0.1991
9	1.8215	0.0446	1.4917	0.1702
11	1.8258	0.0043	1.5401	0.0484
13	1.7648	-0.0610	1.6125	0.0724
15	1.6813	-0.0835	1.6186	0.0061
17	1.4824	-0.1989	1.5728	-0.0458
18	1.6136	0.1312	1.6151	0.0423
Max	1.8258	0.3434	1.6186	0.4962

c-Au NR with an extremely high Δe thus is employed to fabricate helical assemblies in a CLC host to investigate their ability of optical asymmetry magnification. The c-Au NRs with 4 rotational segments and being twisted at $7\pi/2$ exhibit the highest Δe and were helically assembled in a left-handed fashion under the pitches responding to the reflection at the extremely large central wavelength among the typical visible wavelengths. Therefore, a series of helical assemblies as shown in **Fig. 3a** in a CLC host are created for further investigation. The optical asymmetry of thus fabricated helical assemblies is shown in **Fig. 3b,c,d**, and it can be seen that the optical asymmetry of the c-

Au NRs helical assemblies is slightly smaller in comparison to the typical Au NRs helical assemblies. Furthermore, analogous to the optical asymmetric spectra of the typical Au NRs helical assemblies, the specific signals in the extinction spectra, CD spectra and g-factor spectra of c-Au NRs helical assemblies exhibit a blue-shift and an increase in magnitude in response to the incremental incorporation of additional c-Au NRs. In addition to the 5 c-Au NR helical assembly, a maximum blue-shift of longitudinal localized surface polarization resonance (l-LSPR) in extinction spectra of up to 147 nm is observed when the c-Au NRs in the helical assemblies are increased to 18 as shown in **Fig. 3b** and **Table 1**. Meanwhile, the g-factor of the 18 c-Au NR helical assemblies is magnified to a value of 0.606, as shown in **Fig. 3d**. This is attributed to the concomitant reduction in the inter-nanorods spacing within the helical assemblies under the absolute pitch. Moreover, it has been seen that the optical asymmetric signals of c-Au NR helical assemblies exist a slight rightward shift in comparison to those of normal Au NR helical assemblies. In particular, the longitudinal localized surface plasmon resonance (l-LSPR) signal in the extinction spectra of an 18 c-Au NR helical assembly is observed to be located at 1022 nm, exhibiting a red-shift of 181 nm in comparison to the signal observed in the extinction spectra of a normal Au NR helical assembly.

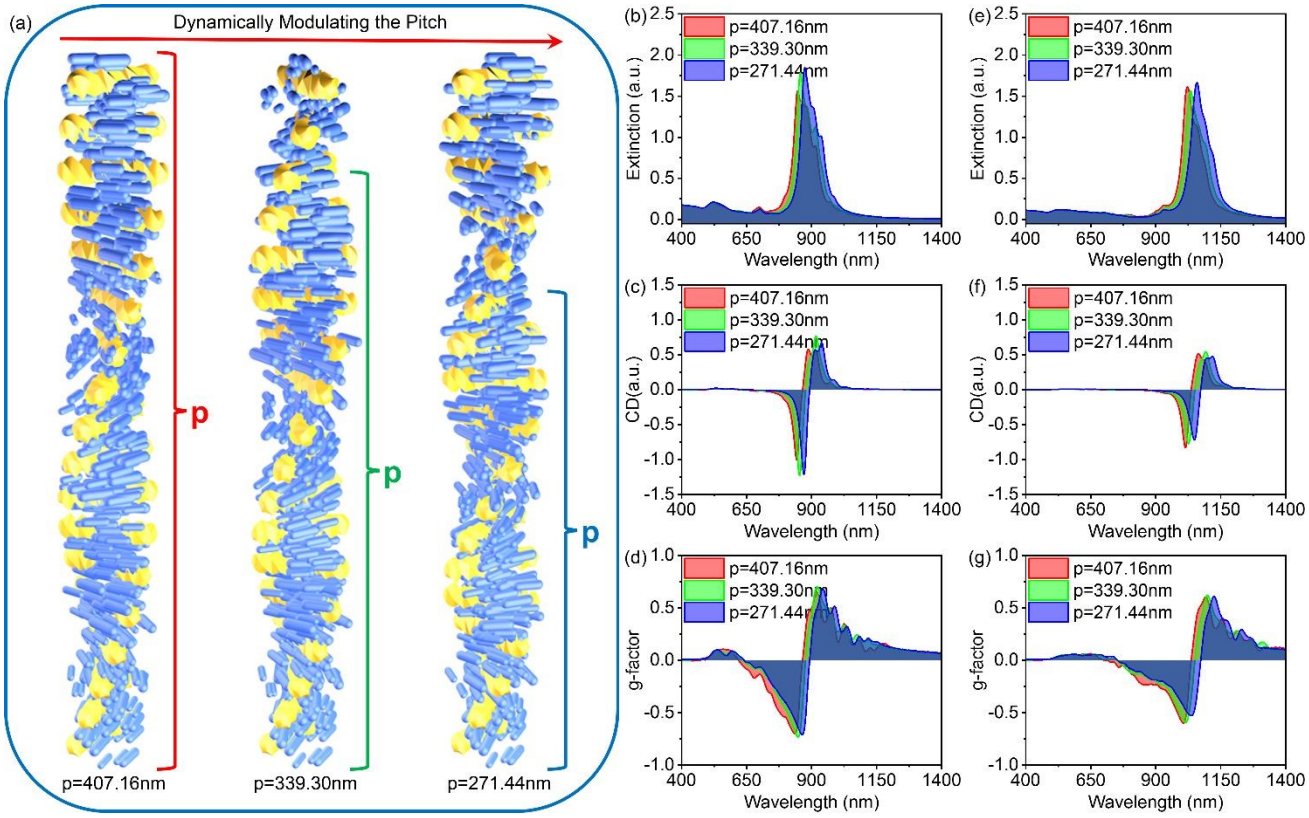

Fig. 4. (a) The schematic illustrates the process of pitch modulation in an 18-c-Au NRs helical assembly with the pitch tuned from 407.16nm to 339.30nm and 271.44nm, respectively. (b) and (e), (c) and (f), (d) and (g) illustrate the change in extinction, CD, and g-factor in response to pitch modification of Au NRs and c-Au NRs helical assemblies, respectively.

The modification of the geometry has a significant impact on the interaction between light and c-Au NRs, which in turn induces a change in the optical asymmetry of the helical assemblies. Herein, the pitch of the helical assembly was modified to 339.36 nm and 257.25 nm, respectively, in comparison to the original 407.16 nm, in order to investigate the impact of geometry on optical asymmetry as shown in **Fig. 4a**. In comparison to the typical Au NRs helical assembly, the negative signals observed in the CD and g-factor spectra as shown in **Fig. 4c,f,d,g** that are indicative of the distinctive l-LSPR signals in the extinction spectra (**Fig. 4b,e**) decrease in intensity and shift to a longer wavelength in response to the modification of pitch. By tuning the pitch of the c-Au NRs helical assembly

to 252.30 nm from 407.16 nm, a reduction of 12.06% in the g-factor has been achieved, compared with the change of typical Au NRs of 4.36%. This evidence substantiates that the intrinsic chirality of Au NRs represents one of the efficacious features that endow the helical assembly with geometry-dependent optical asymmetry. Furthermore, it can be demonstrated that the optical asymmetry of the c-Au NRs helical assembly can be significantly altered by modifying the pitch of the helical assembly.

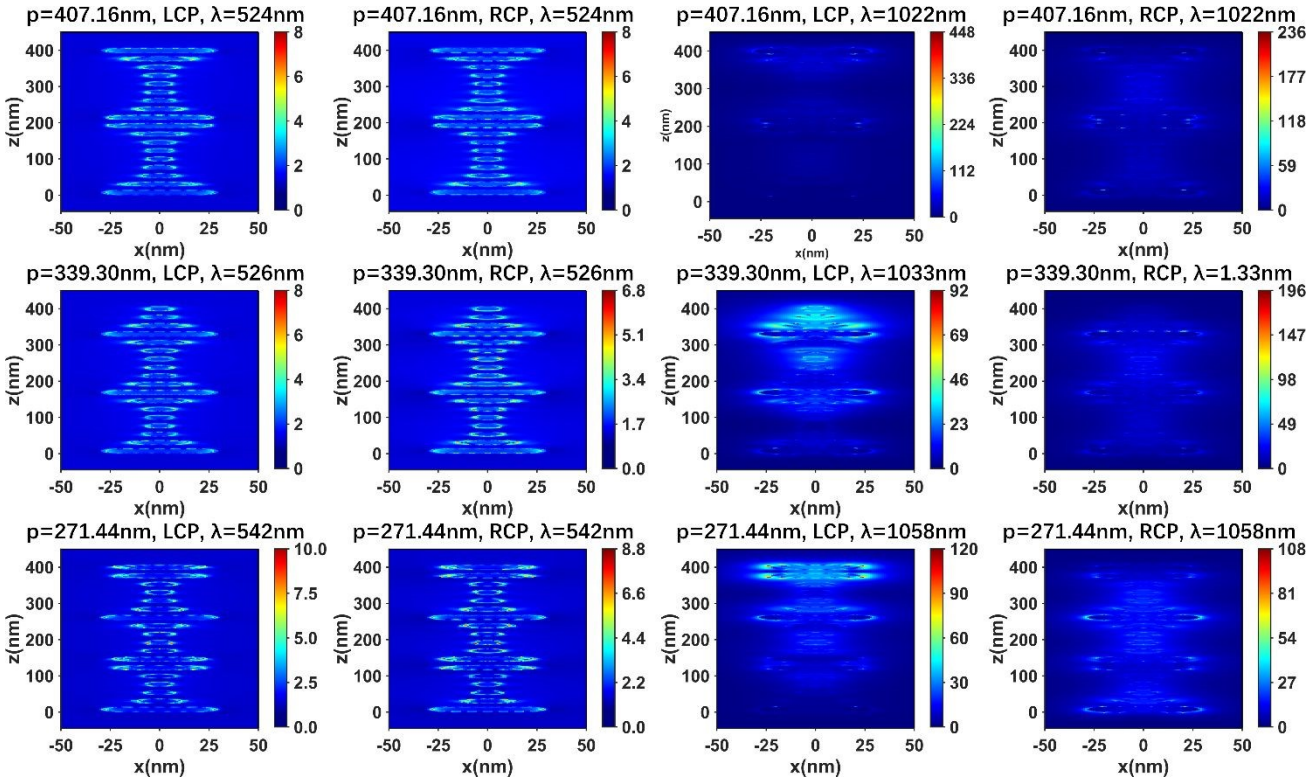

Fig. 5. NFEDs profiles of the 18 c-Au NRs helical assemblies were subjected to pitch modulation under illumination with LCP and RCP light at the corresponding wavelengths of t-LSPR and l-LSPR modes, respectively.

A salient optical property of metal nanoparticles is their capacity for substantial local electromagnetic field enhancement. The underlying physical principle pertains to the phenomenon of surface plasmon resonance (SPR) in metal nanoparticles when exposed to incident light. This interaction gives rise to the generation of a strong electromagnetic field in the immediate vicinity of the particles, leading to the formation of what is commonly referred to as "hot spots". As demonstrated in **Fig. 5**, when the helical assemblies were exposed to the wavelengths of the t-LSPR modes, their near-field enhancement distributions (NFEDs) were found to be indistinguishable under illumination. This finding is analogous to that observed in Au NRs helical assemblies, as reported in the existing literature, and indicates that the field distribution was the same in both the near-field and far-field under LCP and RCP light excitation. In contrast to the NFEDs of Au NRs helical assemblies as shown in **Fig. S3**, which exhibited significant asymmetries in both distribution and magnitude under LCP and RCP light excitation, the c-Au NRs helical assemblies demonstrated a notable similarity in their NFEDs under illumination at the wavelengths of the l-LSPR modes. It was additionally found that the field enhancement is not limited to a few hot spots, but covers a wider range in three-dimensional space. In comparison to normal Au NRs, the intrinsic chirality of c-Au NRs stems from their geometric asymmetry, which lacks mirror symmetry when rotated or translated, inducing a chiral optical response. These responses directly modulate the distribution of electromagnetic fields. Importantly, this chirality introduces phase gradients in the near-field distribution, thereby altering the conditions for constructive interference and hot spot generation. In c-Au NR helical assemblies, asymmetric inter-nanorod spacing or twist angles lead to directional field enhancement along specific axes. Consequently, hot spots are localized at chiral 'hinge' regions

rather than at symmetric midpoints, a spatial bias governed by chiral dipole–dipole interactions, whereby phase mismatch between mirror-image configurations suppresses the formation of symmetric hot spots. Furthermore, in hierarchical c-Au NR assemblies, the intrinsic chirality at each scale modulates the local field enhancement. This results in hot spot distributions that cascade across length scales, generating complex spatial patterns that are unattainable with normal Au NRs helical assemblies. The uniform enhancement of the field allows for light-matter iterations at varying positions, while the extensive field effect serves to mitigate the dissipation triggered by the surface plasmon resonance phenomenon induced by incident light on c-Au NRs. Consequently, this process has been shown to establish a higher modulable optical asymmetry [32].

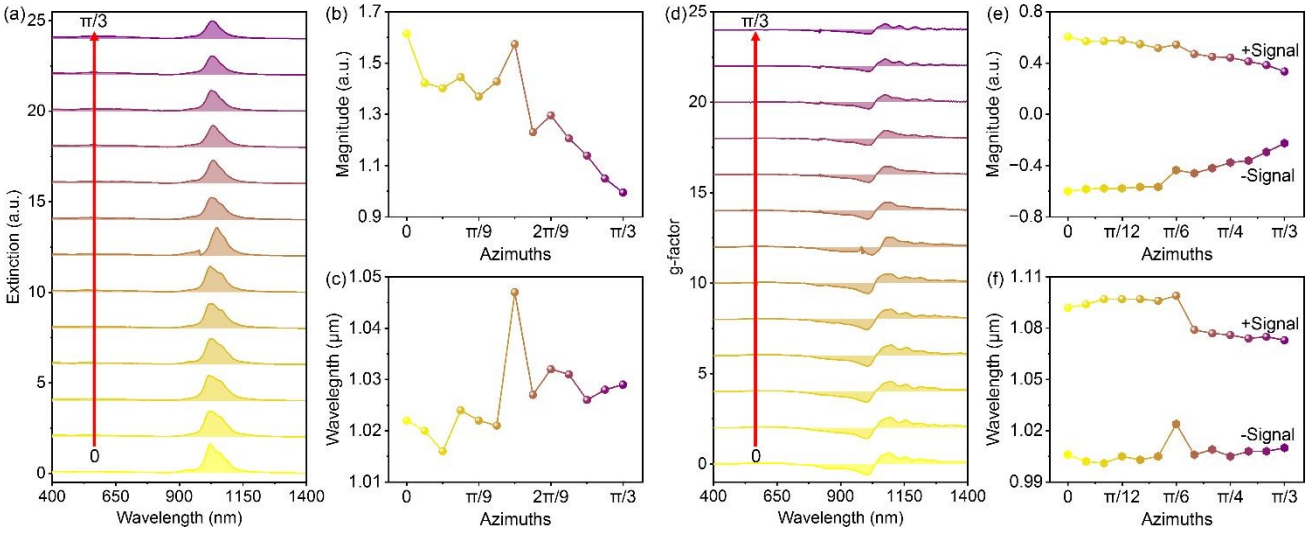

Fig. 6. The optical asymmetry changes in an 18 c-Au NRs helical assembly with a pitch of 407.16nm at different azimuths of helical axis. (a) The extinction spectra changes and the corresponding changes observed from the (b) magnitude and (c) wavelength of l-LSPR signals. (d) The g-factor changes and the corresponding changes observed from the (e) magnitude and (f) wavelength of the bisignate signals.

Table 2. The magnitude changes of the positive signals in the g-factor spectra of an 18 c-Au NRs helical assembly with a pitch of 407.16nm at different azimuths of helical axis.

Helical Assembly	Au NRs		c-Au NRs	
	g-factor	△	g-factor	△
0	0.647	NA	0.606	NA
π/36	0.660	0.013	0.570	-0.036
π/18	0.640	-0.020	0.572	0.002
π/12	0.660	0.021	0.576	0.004
π/9	0.651	-0.009	0.547	-0.029
5π/36	0.679	0.028	0.517	-0.030
π/6	0.675	-0.004	0.545	0.028
7π/36	0.672	-0.003	0.471	-0.074
2π/9	0.594	-0.078	0.449	-0.022
π/4	0.590	-0.004	0.443	-0.006
5π/18	0.588	-0.002	0.412	-0.031
11π/36	0.563	-0.025	0.385	-0.027
π/3	0.542	-0.021	0.335	-0.050

The azimuthal variation-dependent optical asymmetry has been observed in helical assemblies of gold nanoparticles

on DNA origami [33]. However, in our previous study, we observed that the optical asymmetry of typical Au NRs helical assemblies exhibited a relatively constant dependence on the azimuthal variation of helical assemblies within a 0-π/6 range, and the azimuthal variation-induced g-factor curves demonstrated a consistent wavelength dependence without discernible change in visible magnitude. This is primarily attributable to the discrepancy in asymmetries between the helical assemblies and the polarizing light field, which is a consequence of azimuthal variation. Herein, the azimuthal variation has been increased up to π/3 and the optical asymmetry change of helical assemblies is recorded and compared as shown in **Fig. 6 and Fig. S4**. By maintaining a continuous orientation of the azimuthal axis of the typical Au NRs helical assembly from π/6, it was observed that the magnitude of the extinction signals (**Fig. 6a,b**), CD signals (**Fig. S4a,b**), and the bisignate signals in the g-factor spectra (**Fig. 6d,e**) were significantly reduced, but the wavelengths of the signals remained almost at their initial location as shown in **Fig. 6c,f** and **Fig S4c**. Upon reaching an azimuthal variation of π/3, a notable change of 0.271 in the magnitude of the negative signal as shown in **Fig. 6d,e** in the g-factor spectra was observed. In comparison to typical Au NRs helical assemblies, the dependence of the g-factor on azimuthal variation in c-Au NRs helical assemblies is significantly amplified by intrinsic chirality. It is evident that both the bisignate signals in the g-factor spectra are significantly altered by a π/6 azimuthal variation as shown in **Fig. 6e**, indicating that a considerably larger modulation range has been attained. Moreover, in comparation to typical c-Au NRs helical assemblies, the azimuthal variation induced much even greater changes regarding bisignate signals in g-factor spectra, and the change data of the positive signal are shown in **Table 2**. It can be seen from **Table 2** that, although the initial g-factor of c-Au NR is smaller than that of Au NR, the relative change of g-factor of c-Au NR is larger than that of Au NR during the gradual change from 0 to π/3 azimuth. Upon reaching an azimuthal variation of π/3 for the c-Au NRs, a change of 0.271 and 0.137 in the magnitudes of the aforementioned signals in the g-factor spectra was observed, indicating that the intrinsic chirality on Au NRs has induced an overall azimuthal axis-dependent optical asymmetry in the helical assembly, and shows a better optical asymmetry modulation effect in the azimuth dynamic change.

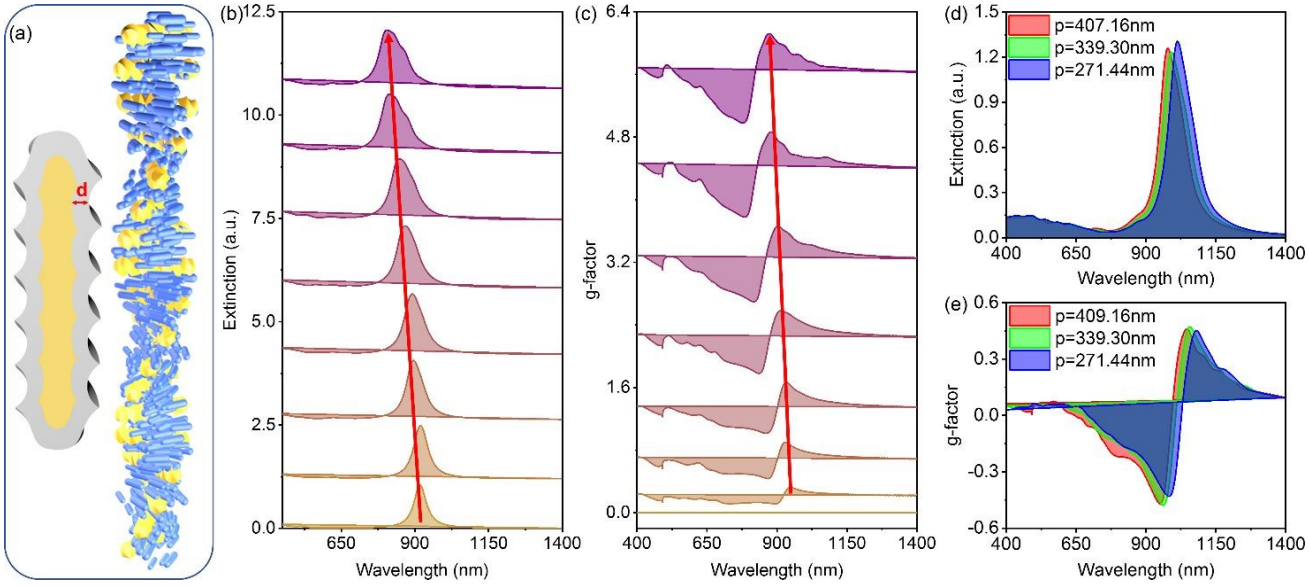

Fig. 7. (a) The schematic of an 56nm×15nm (aspect ratio by 3.73) c-Ag@Au NR and an 18 c-Ag@Au NRs helical assembly in CLC host. (b) and (c) are the changes in the extinction and g-factor of c-Ag@Au NRs helical assembly that are caused by incorporating c-Au NRs into the helical assembly by 5, 7, 9, 11, 13, 15, 17, 18, respectively. (d) and (e) illustrate the changes in extinction and g-factor in response to pitch modification of the 18 c-Ag@Au NRs helical assembly from 407.16nm to 339.30nm and 271.44nm, respectively.

In comparison to Au NRs, Ag@Au NRs with a silver shell (Ag-shell) are reported to have the blue-shifted extinction characteristics, and are believed to have advanced applications within the UV-Vis wavelength. Herein, c-Ag@Au

NRs with a fixed length and diameter of 56 nm and 15 nm, respectively, have been employed for helical assembly construction. Prior to the construction of the c-Ag@Au NRs helical assemblies, a comprehensive examination of the thickness of the Ag-shell was conducted, and the results indicated a significant impact on the extinction performance. As demonstrated in **Fig. S5a**, the LSPR and TSPR signals in the extinction spectra are substantially diminished as the diameter of the Au NR is reduced, while the thickness of the Ag-shell is increased. This phenomenon can be attributed to the fact that the local surface plasmon resonance nature of gold is more pronounced than that of silver. The extinction anisotropy of the c-Ag@Au NRs was screened by equation 2, and it was found that the highest extinction anisotropy at ~0.153 was achieved when the thickness of the Ag-shell reached 4 nm as evidenced in **Fig. S5b**. In parallel with the c-Au NRs helical assemblies as shown in **Fig. 4**, c-Ag@Au NRs helical assemblies were constructed and the optical asymmetric performance of the helical assemblies was investigated, as illustrated in **Fig. 7a,b,c** and **Fig. S7**. In comparison to Au NRs helical assemblies, a significant blue-shift of the optical asymmetric spectra has been observed from c-Ag@Au NRs helical assemblies, and the intensity of the extinction signal, CD signal and g-factor signal all diminished a lot. It is noteworthy that the blue-shift of the signals, induced by the diminution of the inter-nanorods space, has been facilitated by the Ag-shell. This is evidenced by the l-LSPR signal blue-shifting by approximately 58 nm in comparison to the 49 nm shift observed in the c-Au NRs assemblies. In addition to the optical asymmetry change subjected to the pitch modulation, it could be seen from **Fig. 7d,e** that the g-factor has been originally located at 0.4608 when the p=407.16nm, turned to 0.4 714 when the pitch was 339.30nm and became 0.4513 when the pitch was 271.44nm, respectively. This indicates a modulation range of g-factor by 4.26% in c-Ag@Au NRs helical assembly, which thus drives to a conclusion that the Ag-shell diminished the optical asymmetry of helical assembly. In terms of light-matter interaction, similar to c-Au NRs helical assemblies, both c-Ag@Au NRs helical assemblies exhibited analogous NFEDs in response to the exposed circularly polarized light at the t-LSPR wavelength, irrespective of the chirality of the light as shown in **Fig. S6**. However, when the helical assemblies were exposed at the l-LSPR wavelength, the c-Ag@Au NRs helical assembly exhibited brighter NFEDs and was distinguishable from the c-Au NRs helical assembly, indicating that thus the tunable optical asymmetry has been reduced. The response difference between c-Ag@Au NRs helical assemblies and c-Au NRs helical assemblies under the irradiation at their l-LSPR wavelength is attributed to the stability of the c-Ag shell plasmon mode due to its low dissipation [34-36], and the coupling between the c-Au core and c-Ag shell leads to the passivation of photon trapping and a decrease in LSPR.

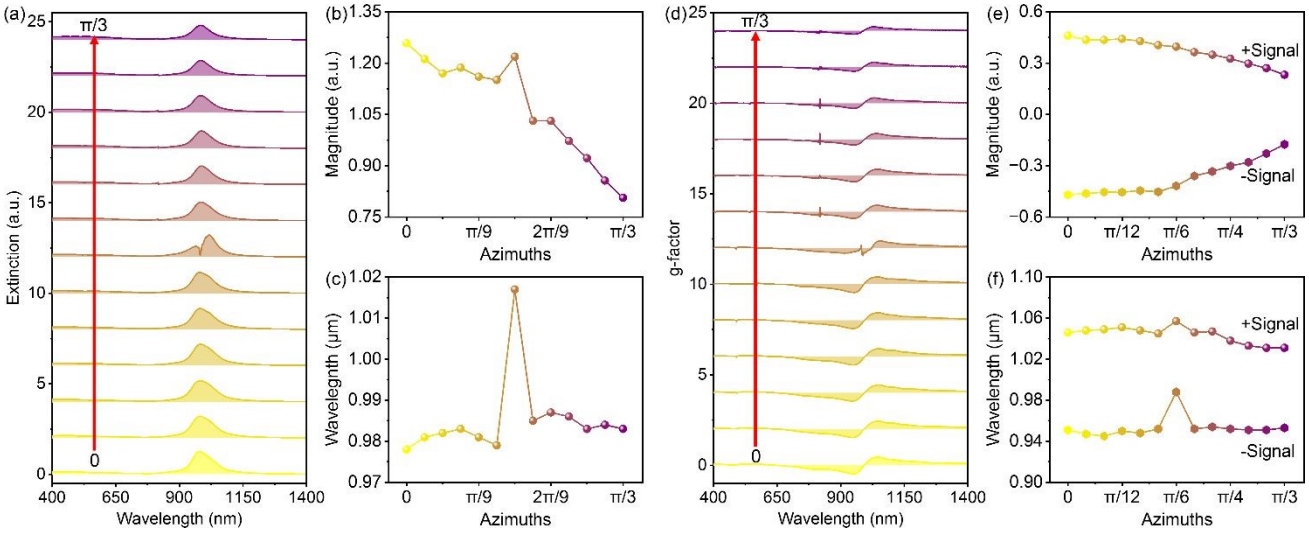

Fig. 8. The optical asymmetry changes in an 18 c-Ag@Au NRs helical assembly with a pitch of 407.16nm at different azimuths of helical axis. (a) The extinction spectra changes and the corresponding changes observed from the (b) magnitude and (c) wavelength of l-LSPR signals. (d) The g-factor changes and the corresponding changes observed from the (e) magnitude and (f) wavelength of the bisignate signals.

Table 3. The magnitude changes of the positive signals in the g-factor spectra of an 18 c-Ag@Au NRs helical assembly with a pitch of 407.16nm at different azimuths of helical axis.

Helical Assembly	c-Au NRs		c-Ag@Au NRs	
	g-factor	△	g-factor	△
0	0.606	NA	0.461	NA
π/36	0.570	-0.036	0.436	-0.025
π/18	0.572	0.002	0.436	0.000
π/12	0.576	0.004	0.442	0.006
π/9	0.547	-0.029	0.429	-0.013
5π/36	0.517	-0.030	0.405	-0.024
π/6	0.545	0.028	0.395	-0.010
7π/36	0.471	-0.074	0.364	-0.031
2π/9	0.449	-0.022	0.349	-0.015
π/4	0.443	-0.006	0.326	-0.023
5π/18	0.412	-0.031	0.297	-0.029
11π/36	0.385	-0.027	0.270	-0.027
π/3	0.335	-0.050	0.232	-0.038

In addition to the optical asymmetry of the c-Ag@Au NRs helical assemblies, it was found that both extinction and the g-factor are much weaker, and their azimuth of helical axis-dependent optical asymmetry exists over a much smaller modulation range in comparison to the c-Au NRs helical assemblies, as illustrated in **Fig. 8 and Fig. S9**. In a similar manner, a reduction in the magnitude of the extinction signals (**Fig. 8a,b**), CD signals (**Fig. S9a,b**), and the bisignate signals in the g-factor spectra (**Fig. 8d,e**) were clearly observed, and the wavelengths of the signals remained almost at their initial location as shown in **Fig. 8c,f** and **Fig S9c**, during the continuous orientation of the azimuthal axis of the typical c-Ag@Au NRs helical assembly until π/3. The original g-factor of c-Ag@Au NRs helical assemblies was found to be 0.461, which decreased by 0.145 in comparison to that of c-Au NRs helical assemblies as shown in **Table 3**. Furthermore, during the azimuthal variation from 0 to π/3, a notable change of 0.229 in the magnitude of the negative signal in the g-factor spectra was observed (see **Fig. 8d,e**), which is a decrease of more than 30% in comparison to the modulation range of c-Au NRs helical assemblies. These observations indicate that the reduced extinction anisotropy by the Ag shell has passivated the light-helical assembly interaction, and that the core Au NRs dominate the response of the c-Ag@Au NRs helical assemblies with optical anisotropy modulation. Furthermore, we investigated the alterations in the optical asymmetries of the c-Au NRs helical assemblies by varying turns and azimuthal angles with the findings illustrated in **Fig. S10**, **Fig. 9** and **Fig. S11**. As shown in **Fig. S10a**, it can be seen that with an increase in the number of helical turns, both the t-LSPR and l-LSPR signals in the extinction spectrum demonstrate a gradual rise, accompanied by a significant broadening and suppression of the signals. The amplitudes of the signals in response to the helical assemblies with three and five turns are approximately three and five times higher, respectively, than that observed at one turn. This is due to the fact that the shielding effect of the stacked c-Au NRs in helical assemblies with increasing turns significantly enhances their extinction response to incident light. In comparison to the signals in the extinction spectra, the bisignate signals in the CD spectra reached a maximum when the number of turns was increased to 3 as shown in **Fig. S10b**. It was also found that the subsequently continuous growth of the turn in the helical assemblies resulted in a decline in the amplitude of the bisignate signals, which is attributed to a reduction in the flux of the irradiating polarized light as evidenced by the extinction characteristics. Additionally, the g-factor was also seen to decrease with an increase in the number of turns as shown in **Fig. S10c**.

The optical asymmetry of helical assemblies was found to be contingent upon the orientation of the helical axis as

shown in Fig. 9 and Fig. S11. The rotation of the helical axis of the three-turn assembly resulted in a slight reduction in extinction, accompanied by an initial decline in the CD signals and g-factors followed by a lateral increase as depicted in Fig. 9a-f and Fig. S11a-c. This demonstrates that the optical asymmetry of the c-Au NRs helical assemblies can function as a mechanism for dynamical tunability beyond that observed in Au NRs. A detailed examination of the g-factor changes reveals that the alteration in g-factor in response to the helical axis orientation alternation from 0 to 7π/36 is as significant as 47.72% spanning a range from -0.505 to 0.264 as shown in Table 4. In comparison to the three-turn helical assembly, the orientation of the helical axis of the five-turn assembly induced a notable increase in extinction, CD, and g-factor as shown in Fig. 9g-l and Fig. S11d-f. However, the region in which the g-factor undergoes dynamical change has been reduced. The aforementioned observations illustrate that super helical assemblies comprising a considerable number of c-Au NRs have induced additional features of dynamically tunable optical asymmetry, superimposed upon the alternation in helical axis orientation.

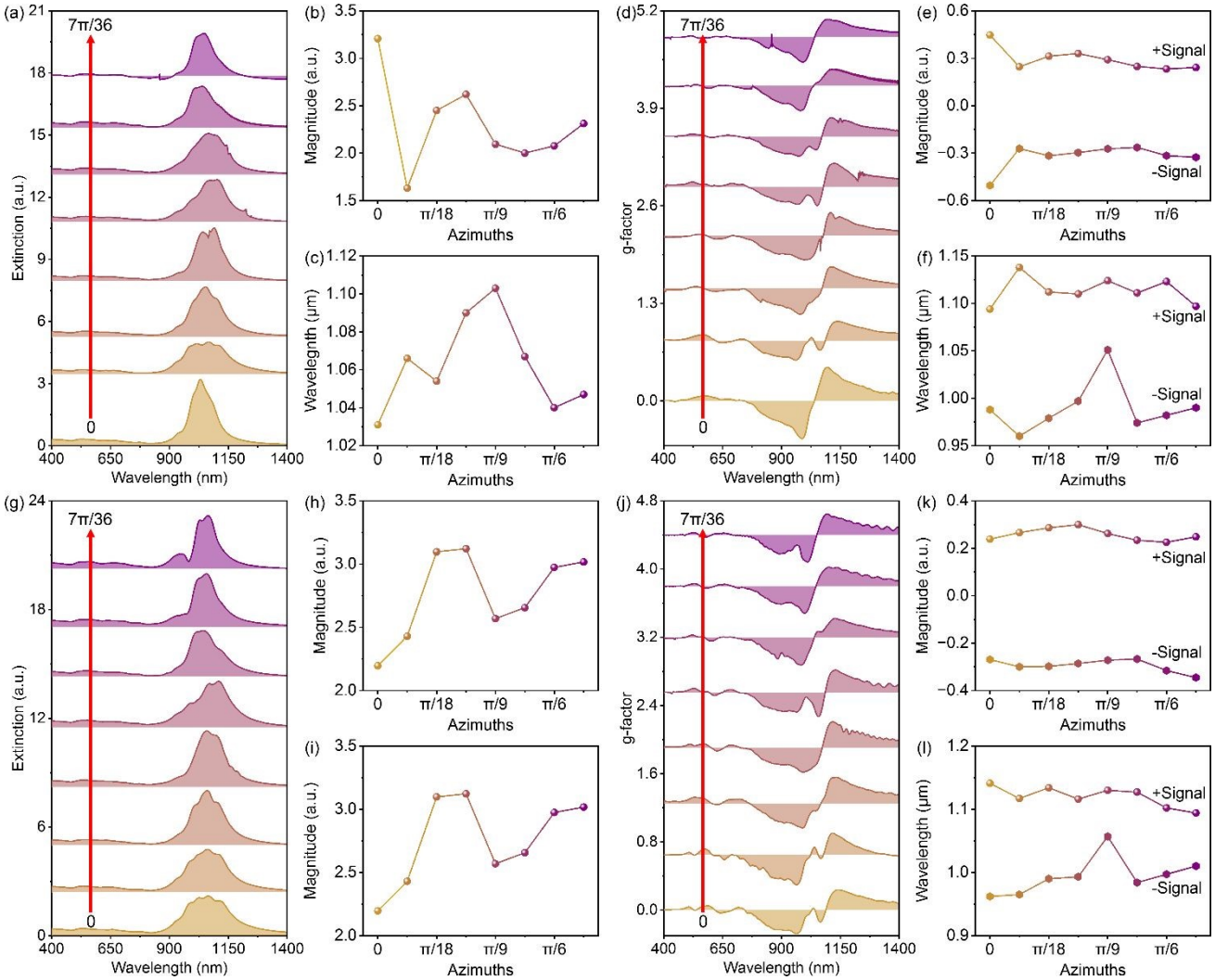

Fig. 9. The optical asymmetry changes of 18 c-Au NRs helical assemblies with a pitch of 407.16nm in 3 turns and 5 turns, respectively, at different azimuths of the helical axis. (a) The extinction spectra changes and the corresponding changes observed from the (b) magnitude and (c) wavelength of l-LSPR signals in 3 turns helical assemblies. (d) The g-factor changes and the corresponding changes observed from the (e) magnitude and (f) wavelength of the bisignate signals in 3 turns helical assemblies. (g) The extinction spectra changes and the corresponding changes observed from the (h) magnitude and (i) wavelength of l-LSPR signals in 5 turns helical assemblies. (j) The g-factor changes and the corresponding changes observed from the (k) magnitude and (l) wavelength of the bisignate signals in 5 turns helical assemblies.

Table 4. The magnitude changes of the positive signals in the g-factor spectra of an 18 c-Ag@Au NRs helical assembly with a pitch of 407.16nm at different azimuths of helical axis and turns.

Helical Assembly	1 Turn		3 Turns		5 Turns	
	g-factor	△	g-factor	△	g-factor	△
0	-0.600	NA	-0.505	NA	-0.269	NA
π/36	-0.583	0.017	-0.271	0.234	-0.300	-0.031
π/18	-0.577	0.006	-0.317	-0.046	-0.298	0.002
π/12	-0.577	0.000	-0.297	0.020	-0.286	0.012
π/9	-0.567	0.010	-0.273	0.024	-0.272	0.014
5π/36	-0.566	0.001	-0.264	0.009	-0.267	0.005
π/6	-0.435	0.131	-0.316	-0.052	-0.316	-0.049
7π/36	-0.460	-0.024	-0.326	-0.010	-0.346	-0.030
0jiantou7π/36	0.140		0.179		0.077	

Conclusion

Interplay between intrinsic chirality and engineered hot-spot spatial arrangements in c-Au NR helical assemblies constitutes a significant research frontier, bridging fundamental plasmonic and applied sensing. Understanding how structural asymmetry dictates near-field localization enables unprecedented control over light–matter interactions, driving innovations in enantioselective sensing, multiplexed detection, and integrated chiral photonics. We emphasize that helically redistributed near-field enhancements-induced by intrinsic chirality-are optimally suited for chiral-selective plasmonic sensing when resonantly coupled to analyte responses, as demonstrated by enantioselective detection in twisted plasmonic lattices and superlattice-based meta-surfaces. Furthermore, embedding c-Au NR helical assemblies within CLC-hosts establishes a versatile modulation platform. This system leverages the inherent dynamic geometric reconfigurability of the helical assemblies within CLCs to amplify and manipulate geometry-dependent optical asymmetry, thereby enabling precise phase and amplitude control of optical signals. These findings collectively support the applicability of such architectures in next-generation sensing and photonic integration platforms. This work has clearly demonstrated a specific example of constructing Au NRs in a CLC host with the widely tunable optical asymmetry. Prior to the theoretical investigation on helical assembly, a selection law of the appropriate Au NR in correlation with extinction characteristics to enlarge the modulation range of optical asymmetry in helical assemblies has been demonstrated. This factor has been named extinction anisotropy factor-Δe, and strongly dependents on the magnitudes of extinctive signals. According to this selection law, in this research the most suitable Au NR for constructing the helical assembly with a wide dynamical modulation range of optical asymmetry was identified as a c-Au NR with 4 rotational segments and being twisted by 7π/2. During the optical asymmetry investigation, the c-Au NRs helical assembly exhibits red-shifted optical asymmetric behavior, which contains 18 NRs at the pitch of 407.16 nm, in comparison to the normal Au NRs helical assembly, and the magnitude of the signals has been found to decrease slightly. Despite these changes, the dynamical modulation change of g-factor in responding to the pitch and azimuthal variation has been found to be surprisingly extended. A 5.3% expansion of modulation range in g-factor was observed when the pitch of the c-Au NRs helical assembly was reduced to 339.30 nm (in comparation to the original base at the pitch of 407.16 nm), and a further extension to the modulation range of g-factor was achieved by 12.06% when the pitch of the c-Au NRs helical assembly was reduced to 252.30 nm, indicating 3 times larger than that of normal Au NRs helical assembly. Furthermore, the helical axis of the c-Au NRs helical assembly was tuned from 0 to π/3 resulted in a 0.271 change in g-factor. This indicates an expanded modulation range of 44.72% at its original base. Ag shell is sufficient to resist the red-shift of optical asymmetric signals; however, this also leads to a decrease in the magnitude of signals, primarily due to the extinctive characteristic difference between the Au core and the Ag shell. Moreover, by increasing the helical turns of

View Article Online
DOI: 10.1039/D5TC02438B

assemblies to 3, the optical asymmetric signals dominate the highest value, and a modulation of g-factor by 0.179 when the azimuths of helical assembly was tuned from 0 to 7π/36. The superiority of c-Au NR in magnifying optical asymmetry modulation has been also approved in head-by head assemblies, in which the modulation range of g-factor has been confirmed as 0.321, indicating an expansion of 21% in comparison to that of normal Au NRs helical assembly. The findings in this research indicate a possible way to construct helical assembly with a wide and tunable optical asymmetry, and the example of helical assemblies constructed here greatly approved our proposed Au NR selection law and our estimation. The findings in this research indicate a possible way to construct helical assembly with a wide and tunable optical asymmetry, and the example of helical assemblies constructed here greatly approved our proposed Au NR selection law and our estimation, and our future work will prioritize atomistic simulations of NFEDs coupling and scalable fabrication techniques to translate these concepts into practical devices.

Experiment

c-Au NRs Helical Assemblies Modeling: A novel approach to modelling intrinsic c-Au NRs (aspect ratio by 3.73, 56 nm in length ×15 nm in diameter) in simulation by twist angle and the rotation segment is proposed here, which differs from the conventional approach adopted to date [29, 37]. Specifically, in the course of the investigation of isolated c-Au NR in C4D (R20, Maxon Computer Gmbh, Germany), it was established that the twist angle changes from 0 to 5π, and the rotation segments are in the range from 4 to 25.

The hypothesis is that c-Au NRs self-assemble helically within a CLC host under the pitch of 407.16 nm, analogous to the assembly of LC molecules in a side by side fashion as indicated by experimental results obtained previously [26]. It is anticipated that these helical assemblies of c-Au NRs will possess an identical pitch to that of the CLC host, thereby giving rise to a pitch variation amongst the c-Au NRs helical assemblies in conjunction with the stimuli-induced dynamical changes of the CLC host. However, during the process of dynamic pitch tuning, the inter-nanorods distance between the c-Au NRs remains at the initial gap, as it can only be modified by varying the blending concentration.

Finite difference time domain (FDTD) simulations: In FDTD simulation (8.15.736 Linux, Lumerical FDTD Solutions, Canada), two Total Field Scattered Field (TFSF) light sources, generating circular polarization, were positioned vertically above the helical assemblies of c-Au-NRs. The vibration planes of the two light beams were perpendicularly arranged, thereby illuminating the geometric center of the c-Au-NRs helical assemblies along the negative Z-axis. In order to achieve left-handed or right-handed circularly polarized light (LCPL and RCPL), one of the light beams must be shifted by π/2 or -π/2 in its phase, respectively. It is recommended that the uniform refinement-mesh composed full-field scattered light sources are employed to enhance the accuracy of the simulations. In this instance, a refinement-mesh with a grid resolution of 2 nm in all directions was employed in front of the sources. Extinction spectra, CD spectra and g-factor of the c-Au-NRs helical assemblies were obtained through post-calculations of the recorded absorption and scattering beams by two analysis groups. The simulation region was created based on the varying dimensions of the c-Au-NRs helical assemblies. The XY plane was in periodic boundary condition, but in the Z direction it employed a perfectly matched layer (PML). During the simulations, the background permittivity was maintained at 1.634 (liquid crystal, E7), the temperature was 300 K, and the conformal variant of mesh refinement was set to 0. The simulations were terminated when the field strength in the simulation region dropped to 1e-6 or when the maximum simulation time of 3500 femtoseconds was reached.

Funding. This work was supported by the National Natural Science Foundation of China (62241503), the Natural Science Foundation of Shanghai (22ZR1401400).

Data availability. The data supporting this article have been included as part of the Supplementary Information.

Disclosures. The authors declare no conflicts of interest.

References

[1]. Knoppe, S.; Bürgi, T. Chirality in Thiolate-Protected Gold Clusters. Acc. Chem. Res. 2014, 47 (4), 1318–1326. DOI: 10.1021/ar400295d

[2]. Oh, S. S.; Demetriadou, A.; Wuestner, S.; Hess, O. On the Origin of Chirality in Nanoplasmonic Gyroid Metamaterials. Adv. Mater. 2013, 25 (4), 612-617. DOI: 10.1002/adma.201202788

[3]. Ben-Moshe, A.; Maoz, B.; Govorov, A. O.; Markovich, G. Chirality and Chiroptical Effects in Inorganic Nanocrystal Systems with Plasmon and Exciton Resonances. Chem. Soc. Rev. 2013, 42 (16), 7028-7041, DOI: 10.1039/c3cs60139k

[4]. Choi, J.-H.; Hwang, H. S.; Jang, H.-B.; Kim, S.-U.; Park, H.-L. Flexible Phototransistors Integrated with Chiral Liquid Crystal Encapsulating Film for Improving Color Selectivity and Stability. ACS Appl. Electron. Mater. 2024, 6 (11), 8094-8103. DOI: 10.1021/acsaelm.4c01439

[5]. Peluso, P.; Chankvetadze, B. Recognition in the Domain of Molecular Chirality: From Noncovalent Interactions to Separation of Enantiomers. Chem. Rev. 2022, 122 (16), 13235-13400. DOI: 10.1021/acs.chemrev.1c00846

[6]. Nishino, T.; Umezawa, Y. Single-Molecule Chiral Recognition on a Surface by Chiral Molecular Tips. Anal. Chem. 2008, 80 (18), 6968-6973. DOI: 10.1021/ac800818f

[7]. Hentschel, M.; Schäferling, M.; Duan, X.; Giessen, H.; Liu, N. Chiral Plasmonics. Sci. Adv. 2017, 3 (5), e1602735. DOI: 10.1126/sciadv.1602735

[8]. Liang, J.; Guo, P.; Qin, X.; Gao, X.; Ma, K.; Zhu, X.; Jin, X.; Xu, W.; Jiang, L.; Duan, P. Hierarchically Chiral Lattice Self-Assembly Induced Circularly Polarized Luminescence. ACS Nano 2020, 14 (3) 3190-3198. DOI: 10.1021/acsnano.9b08408

[9]. Sun, X.; Kong, H.; Zhou, Q.; Tsunega, S.; Liu, X.; Yang, H.; Jin, R. Chiral Plasmonic Nanoparticle Assisted Raman Enantioselective Recognition. Anal. Chem. 2020, 92 (12), 8015-8020. DOI: 10.1021/acs.analchem.0c01311

[10]. Yu, P.; Zhao, W.; Huang, Y.; Zeng, H.; Wan, X.; Zhang, J. Edge-directed Rapid Chiral Assembly of Gold Nanorods by 2D Hexagonal Nanosheets of Helical Poly(phenylacetylene)s and the Synergistic Communication of Circularly Polarized Luminescence. J. Mater. Chem. C, 2025,13, 7502-7508. DOI: 10.1039/D5TC00312A

[11]. Zhang, L.; Chen, Y.; Zheng, J.; Lewis, G. R.; Xia, X.; Ringe, E.; Zhang, W.; Wang, J. Chiral Gold Nanorods with Five-Fold Rotational Symmetry and Orientation-Dependent Chiroptical Properties of Their Monomers and Dimers. Angew. Chem. Int. Ed. 2023, 62, e202312615. DOI: 10.1002/anie.202312615

[12]. Thomas, A. R.; Swetha, K.; Aparna, C. K.; Ashraf, R.; Kumar, J.; Kumar, S.; Mandal, S. S. Protein Fibril Assisted Chiral Assembly of Gold Nanorods. J. Mater. Chem. B, 2022,10, 6360-6371. DOI: 10.1039/D2TB01419J

[13]. Lu, X.; Ye, W.; You, W.; Xie, H.; Hang, Z.; Lai, Y.; Ni, W. Collective Resonance in Helical Superstructures of Gold Nanorods. Phys. Rev. 2020, 101 (4), 045431. DOI: 10.1103/PhysRevB.101.045431

[14]. Lan, X.; Lu, X.; Shen, C.; Ke, Y.; Ni, W.; Wang, Q. Au Nanorod Helical Superstructures with Designed Chirality. J. Am. Chem. Soc. 2015, 137 (1), 457-462. DOI: 10.1021/ja511333q

[15]. Wang, R.; Wang, H.; Wu, X.; Ji, Y.; Wang, P.; Qu, Y.; Chung, T.-S.; Chiral Assembly of Gold Nanorods with Collective Plasmonic Circular Dichroism Response. Soft Matter. 2011, 7 (18), 8370-8375. DOI: 10.1039/C1SM05590A

[16]. Lu, J.; Xue, Y.; Bernardino, K.; Zhang, N.-N.; Gomes, W. R.; Ramesar, N. S.; Liu, S.; Hu, Z.; Sun, T.; Farias de Moura, A.; Kotov, N. A.; Liu, K. Enhanced Optical Asymmetry in Supramolecular Chiroplasmonic Assemblies with Long-range Order. Science 2021, 371 (6536), eabd8576. DOI: 10.1126/science.abd8576

[17]. Li, Z.; Zhu, Z.; Liu, W.; Zhou, Y.; Han, B.; Gao, Y.; Tang, Z. Reversible Plasmonic Circular Dichroism of Au

Nanorod and DNA Assemblies. J. Am. Chem. Soc. 2012, 134 (7), 3322-3325. DOI: 10.1021/ja209981n

[18]. Li, H., Meng, D., Zhang, C., Ji, Y., Gao, X.; Hu, Z., Wu, X. Temperature-modulated Inversion and Switching of Chiroptical Responses in Dynamic Side-by-side Oligomers of Gold Nanorods. Nano Res. 2023, 16 (12), 13392–13399. DOI: 10.1007/s12274-023-5985-3

[19]. Zhao, W.; Zhang, W.; Wang, R.-Y.; Ji, Y.; Wu, X.; Zhang, X.; Photocontrollable Chiral Switching and Selection in Self-Assembled Plasmonic Nanostructure. Adv. Funct. Mater. 2019, 29 (20), 1900587. DOI: 10.1002/adfm.201900587

[20]. Meng, D.; Chen, Y.; Ji, Y.; Shi, X.; Wang, H.; Wu, X. Temperature Effect of Plasmonic Circular Dichroism in Dynamic Oligomers of AuNR@Ag Nanorods Driven by Cysteine: The Role of Surface Atom Migration. Adv. Optical Mater. 2021, 9 (2), 2001274. DOI: 10.1002/adom.202001274

[21]. John, N.; Mariamma, A. T. Recent Developments in the Chiroptical Properties of Chiral Plasmonic Gold Nanostructures: Bioanalytical Applications. Microchim Acta 2021, 188 (12), 424. DOI: 10.1007/s00604-021-05066-8

[22]. Wu, Y.; Li, M.; Zheng, Z.-G.; Yu, Z.-Q.; Zhu, W.-H. Liquid Crystal Assembly for Ultra-dissymmetric Circularly Polarized Luminescence and Beyond. J. Am. Chem. Soc. 2023, 145 (24), 12951-12966. DOI: 10.1021/jacs.3c01122

[23]. Chen, S.; Katsonis, N.; Leigh, D. A.; Patanapongpibul, M.; Ryabchun, A.; Zhang, L. Changing Liquid Crystal Helical Pitch with a Reversible Rotaxane Switch. Angew. Chem. Int. Ed. 2024, 63 (18), e202401291. DOI: 10.1002/anie.202401291

[24]. Wang, H.; Bisoyi, H. K.; McConney, M. E.; Urbas, A. M.; Bunning, T. J.; Li, Q. Visible-Light-Induced Self-Organized Helical Superstructure in Orientationally Ordered Fluids. Adv. Mater. 2019, 31 (39), 1902958. DOI: 10.1002/adma.201902958

[25]. Bagiński, M.; Tupikowska, M.; González-Rubio, G.; Wójcik, M.; Lewandowski, W. Shaping Liquid Crystals with Gold Nanoparticles: Helical Assemblies with Tunable and Hierarchical Structures Via Thin-Film Cooperative Interactions. Adv. Mater. 2020, 32 (1), 1904581. DOI: 10.1002/adma.201904581

[26]. Liu, Y.; Lin, G.; Chen, Y.; Wei, X.; Du, M.; Zhang, Y.; Li, Z.; Zhao, L. UV-Triggered Optical Asymmetry Modification of Gold Nanorods Helical Assemblies in a Cholesteric Liquid Crystal Host. Adv. Opt. Mater. 2024, 12 (24), 2400862. DOI: 10.1002/adom.202400862

[27]. Ni, B.; Mychinko, M.; Gómez-Graña, S.; Morales-Vidal, J.; Obelleiro-Liz, M.; Heyvaert, W.; Vila-Liarte, D.; Zhuo, X.; Albrecht, W.; Zheng, G.; González-Rubio, G.; Taboada, J. M.; Obelleiro, F.; López, N.; Pérez-Juste, J.; Pastoriza-Santos, I.; Cölfen, H.; Bals, S.; Liz-Marzán, L. M. Chiral Seeded Growth of Gold Nanorods Into Fourfold Twisted Nanoparticles with Plasmonic Optical Activity. Adv. Mater. 2023, 35, 2208299. DOI: 10.1002/adma.202208299

[28]. González-Rubio, G.; Mosquera, J.; Kumar, V.; Pedrazo-Tardajos, A.; Llombart, P.; Solís, D. M.; Lobato, I.; Noya, E. G.; Guerrero-Martínez, A.; Taboada, J. M.; Obelleiro, F.; MacDowell, L. G.; Bals, S.; Liz-Marzán, L. M. Micelle-directed Chiral Seeded Growth on Anisotropic Gold Nanocrystals. Science 2020, 368, 1472-1477. DOI:10.1126/science.aba0980

[29]. Obelleiro-Liz, M.; Martín, V. F.; Solís, D. M.; Taboada, J. M.; Obelleiro, F.; Liz-Marzán, L. M. Influence of Geometrical Parameters on the Optical Activity of Chiral Gold Nanorods. Adv. Optical Mater. 2023, 11, 2203090. DOI: 10.1002/adom.202203090

[30]. Zhang, N.-N.; Shen, Z.-L.; Gao, S.-Y.; Peng, F.; Cao, Z.-J.; Wang, Y.; Wang, Z.; Zhang, W.; Yang, Y.; Liu, K.; Sun, T. Synthesis and Plasmonic Chiroptical Properties of Double-Helical Gold Nanorod Enantiomers. Adv.

Optical Mater. 2023, 11, 2203119. DOI: 10.1002/adom.202203119

[31]. Zhang, N.-N.; Mychinko, M.; Gao, S.-Y.; Yu, L.; Shen, Z.-L.; Wang, L.; Peng, F.; Wei, Z.; Wang, Z.; Zhang, W.; Zhu, S.; Yang, Y.; Sun, T.; Liz-Marzán, L. M.; Bals, S.; Liu, K. Self-Matching Assembly of Chiral Gold Nanoparticles Leads to High Optical Asymmetry and Sensitive Detection of Adenosine Triphosphate. Nano Lett. 2024, 24(41), 13027-13036. DOI: 10.1021/acs.nanolett.4c03782

[32]. Li, Z.-Y.; Xia, Y. Metal Nanoparticles with Gain toward Single-molecule Detection by Surface-enhanced Raman Scattering. Nano Lett. 2010, 10 (1), 243-249. DOI: 10.1021/nl903409x

[33]. Schreiber, R.; Luong, N.; Fan, Z.; Kuzyk, A.; Nickels, P. C.; Zhang, T.; Smith, D. M.; Yurke, B.; Kuang, W.; Govorov, A. O.; Liedl, T. Chiral Plasmonic DNA Nanostructures with Switchable Circular Dichroism. Nat Commun. 2013, 4, 2948. DOI: 10.1038/ncomms3948

[34]. Maoz, B. M.; Chaikin, Y.; Tesler, A. B.; Bar Elli, O.; Fan, Z.; Govorov, A. O.; Markovich, G. Amplification of Chiroptical Activity of Chiral Biomolecules by Surface Plasmons. Nano Lett. 2013, 13 (3), 1203-1209. DOI: 10.1021/nl304638a

[35]. Steele, J.; Grady, N.; Nordlander, P.; Halas, N. (2007) Surface Plasmon Nanophotonics. In: Brongersma, M.L., Kik, P.G. (eds) Surface Plasmon Nanophotonics. Springer Series in Optical Sciences, Springer, Dordrecht. pp 183–196. DOI: 10.1007/978-1-4020-4333-8_13.

[36]. Qiu, M.; Zhang, L.; Tang, Z.; Jin, W.; Qiu, C.-W.; Lei, D. Y. 3D Metaphotonic Nanostructures with Intrinsic Chirality. Adv. Funct. Mater. 2018, 28 (45), 1803147. DOI: 10.1002/adfm.201803147.

[37]. Fu, W.; Chen, J.; Zhang, S.; Zheng, G.; Zhang, Y. Discrete and Dimeric Chiral Plasmonic Nanorods: Intrinsic Chirality and Extrinsic Chirality. J. Mater. Chem. C. 2024, 12(25), 9139–9145. DOI: 10.1039/D4TC01117A.

View Article Online
DOI: 10.1039/D5TC02438B

- The data supporting this article have been included as part of the Supplementary Information.